

Loss compensation in metal-dielectric structures in negative-refraction and super-resolving regimes

M. A. Vincenti,^{1,2,*} D. de Ceglia,² V. Rondinone,¹ A. Ladisa,¹ A. D’Orazio,¹ M. J. Bloemer,² and M. Scalora²

¹*Dipartimento di Elettrotecnica ed Elettronica, Politecnico di Bari, Via Orabona 4, 70025 Bari, Italy*

²*Charles M. Bowden Research Center, AMSRD-AMR-WS-ST, Redstone Arsenal, Alabama 35898-5000, USA*

(Received 29 July 2009; published 5 November 2009)

We study the influence of gain on negative refraction and super-resolution in transparent resonant metal-dielectric photonic band gap structures in the visible and near infrared ranges. We find that while the introduction of gain can compensate for losses caused by the excitation of surface waves, it also improves the resolving characteristics of the lens and leads to gain-tunable super-resolution.

DOI: [10.1103/PhysRevA.80.053807](https://doi.org/10.1103/PhysRevA.80.053807)

PACS number(s): 42.25.Bs, 42.25.Fx, 42.70.Qs, 42.79.Ag

I. INTRODUCTION

Negative index materials have been shown to possess extraordinary new properties not achievable with other materials in nature, creating new opportunities in all fields of optics. Negative refraction, backward phase propagation, superlensing, and super-guiding are just a few of the effects that have been discussed within just the last few years [1–8]. However, while negative index materials and negative refraction were demonstrated in the microwave regime [9–11], a similar undertaking in the visible range still remains a challenging task. To date, negative index metamaterials have been developed using metallic inclusions in the form of nanorods, nanostrips, or perforated metallic films that suffer from high losses at optical frequencies, significantly frustrating their performance [9–16]. In fact also Pendry’s original proposal [1], which consisted of a single 40-nm-thick silver layer, being able to both focus the propagating components and “amplify” evanescent modes, undergoes a significant degradation of the super-resolution ability due to silver intrinsic losses. Moreover, the frustration of the transparency remains a big issue even for multilayer including relatively thin layers [4], leading researchers to formulate alternative designs of super-resolving systems.

It has already been shown that in the context of nonresonant metal-dielectric stacks the addition of an active medium has the potential of improving super-resolution [17]. The idea there was to circumvent material losses by introducing a material with a dielectric constant with exactly the opposite sign and magnitude as the metal in order to force the “perfect lens” condition. In reality, it has been demonstrated that in resonant stacks the actual operational range of super-resolution for any given stack is not strictly tied to the perfect lens condition and that losses are naturally suppressed by the resonant nature of the multilayer stack [6]. Therefore, under realistic conditions metal absorption is generally not an obstacle, and super-resolution is already obtained across a broad spectral range with relatively high transmittance [3,18,19]. Rather, in resonant structures the issue is to see whether or not the introduction of gain within the dielectric layers alters the relative localization properties of the fields

inside the stack and acts to either disrupt or improve the balance achieved between negative refraction of the Poynting vector inside the metal layer and normal refraction inside the dielectric layers.

The present effort represents the continuation of a previous contribution which was focused on a passive resonant metal-dielectric multilayer [6]. The first objective of this paper is to study the introduction of a gain material inside the transparent metal stack to compensate both linear and plasmonic losses without interfering with the negative refraction of the Poynting vector (the direction of energy flow) and to compare the performance of passive and active multilayer stacks. Our second objective is to explore both the negative-refraction and super-resolving regimes to assess the full impact of the introduction of gain within different kinds of stacks.

II. FINITE-DIFFERENCE TIME-DOMAIN TWO-DIMENSIONAL IMPLEMENTATION OF OPTICAL GAIN

In order to explore the possibility to compensate losses in metal-dielectric photonic band gap (MD-PBG) structure we theoretically considered the introduction of gain material inside the transparent stack. In fact, in the MD-PBGs there are linear losses due to the mere presence of metal, while the excitation of surface plasmons in the superguiding regime causes additional significant losses. All the simulations of both passive and active multilayer stacks were performed with our own two-dimensional finite-difference time-domain (FDTD) method. As reported in several works [20–22], one way to model optical gain in a dielectric material consists of introducing a frequency-dependent Lorentzian negative conductivity as follows:

$$\sigma(\omega) = \frac{J_z(\omega)}{E_z(\omega)} = \frac{1}{1 + \frac{I}{I_s}} \left[\frac{\frac{\sigma_0}{2}}{1 + j(\omega - \omega_0)T_2} + \frac{\frac{\sigma_0}{2}}{1 + j(\omega + \omega_0)T_2} \right], \quad (1)$$

where σ_0 is the maximum value of the conductivity, T_2 is a time constant that defines the spread of the Lorentzian spec-

*vincenti@deemail.poliba.it

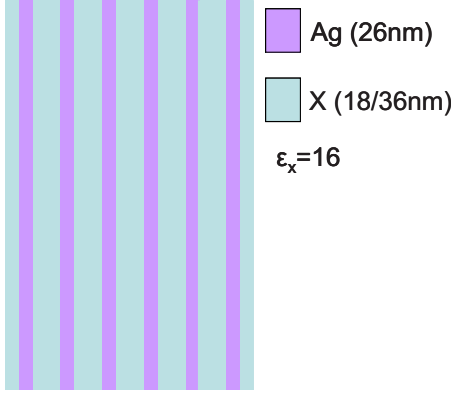


FIG. 1. (Color online) Sketch of the Ag/X multilayer.

tral profile, ω_0 is the resonance frequency, and $S=[1+(I/I_s)]^{-1}$ is the saturation coefficient, where I is the spatially dependent intensity and I_s is the saturation intensity. The choice of a Lorentzian shape for the conductivity is based on the consideration that more complicated or experimental gain spectra can be approximated using a linear combination of Lorentzian curves. Another implicit assumption made is the disregard for the exact nature of the active substance: no interaction between the input signal and other fields (such as the optical pump) is considered. Under these working conditions and further assuming that we are considering linear media in all the simulations, I assumes small values compared to I_s so that the saturation coefficient value is ~ 1 . Equation (1) is then substituted into the electric current density term in Maxwell's equations and discretized as follows [23]:

$$E_x^{n+1}(i,k) = E_x^n(i,k) + \frac{\Delta t}{\epsilon \Delta y} \left[H_z^{n+1/2} \left(i, k + \frac{1}{2} \right) - H_z^{n+1/2} \left(i, k - \frac{1}{2} \right) \right] + - \frac{\Delta t}{2\epsilon} [J_x^{n+1}(i,k) + J_x^n(i,k)], \quad (2a)$$

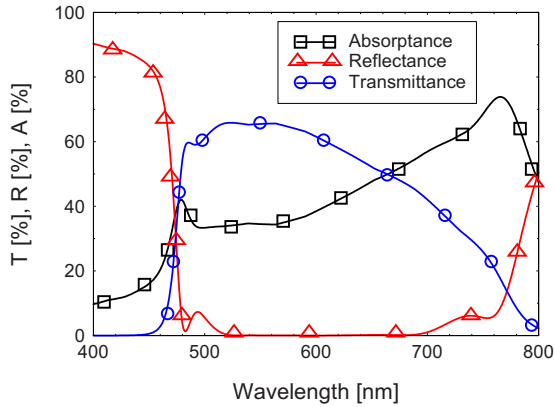


FIG. 2. (Color online) Transmittance (circle markers), reflectance (triangle markers), and absorbance (square markers) spectra of the 5.5 period Ag(26 nm)/X(36 nm) structure at 45° of incidence with respect to the propagation direction. The structure is coated with 18-nm-thick layers of material X ($n=4$).

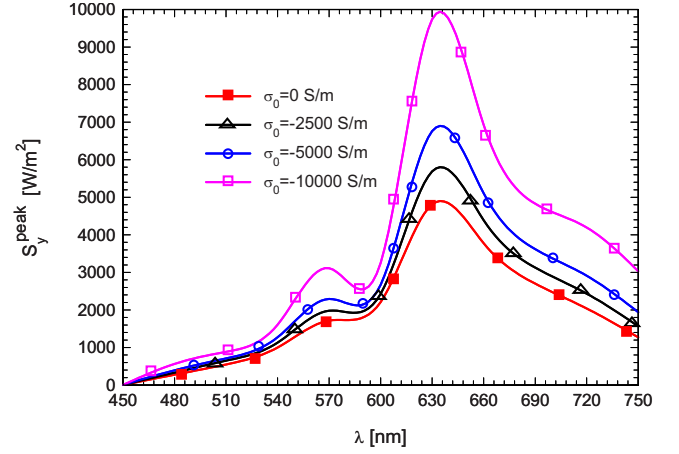


FIG. 3. (Color online) Peak value of the longitudinal Poynting vector at the exit of the stack for different constant gain values.

$$E_y^{n+1}(i,k) = E_y^n(i,k) + \frac{\Delta t}{\epsilon \Delta x} \left[H_z^{n+1/2} \left(i + \frac{1}{2}, k \right) - H_z^{n+1/2} \left(i - \frac{1}{2}, k \right) \right] + - \frac{\Delta t}{2\epsilon} [J_y^{n+1}(i,k) + J_y^n(i,k)], \quad (2b)$$

where

$$J_x^{n+1}(i,k) = J_x^n(i,k) + \frac{\Delta t}{2} [F_x^{n+1}(i,k) + F_x^n(i,k)], \quad (3a)$$

$$J_y^{n+1}(i,k) = J_y^n(i,k) + \frac{\Delta t}{2} [F_y^{n+1}(i,k) + F_y^n(i,k)] \quad (3b)$$

and

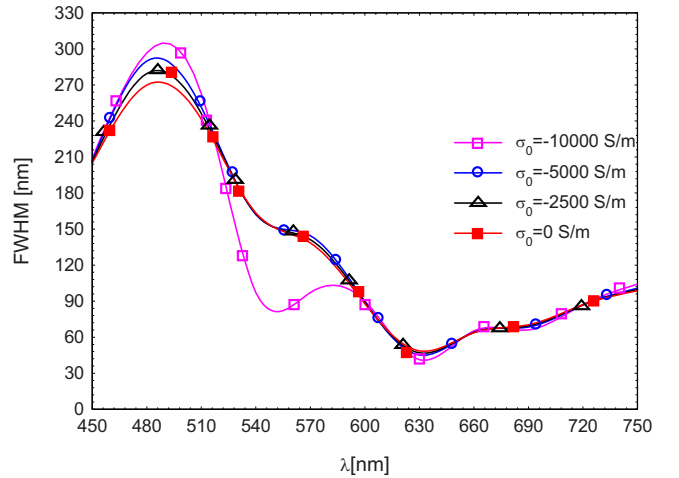


FIG. 4. (Color online) FWHM of the longitudinal Poynting vector at the exit of the stack as a function of the incident wavelength. Values of σ_0 beyond $-10\,000$ S/m result in the boost of the diffraction process since the balance of positive and negative refractions inside the stack is not more preserved.

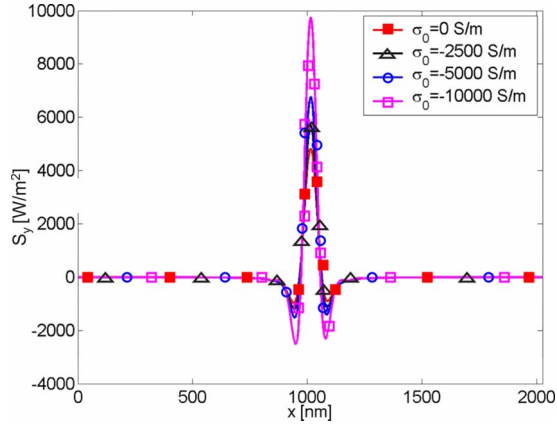


FIG. 5. (Color online) Longitudinal Pointing vector profile at the exit of the stack for different constant gain values and an incident wavelength $\lambda=630$ nm.

$$F_x^{n+1}(i,k) = A_{1x}(i,k) \left[H_z^{n+1/2}(i,k + \frac{1}{2}) - H_z^{n+1/2}(i,k - \frac{1}{2}) \right] + A_{2x}(i,k) E_x^n(i,k) + A_{3x}(i,k) J_x^n(i,k) + A_{4x}(i,k) F_x^n(i,k), \quad (4a)$$

$$F_y^{n+1}(i,k) = A_{1y}(i,k) \left[H_z^{n+1/2}(i + \frac{1}{2},k) - H_z^{n+1/2}(i - \frac{1}{2},k) \right] + A_{2y}(i,k) E_y^n(i,k) + A_{3y}(i,k) J_y^n(i,k) + A_{4y}(i,k) F_y^n(i,k). \quad (4b)$$

Here the coefficient A_{1x} , A_{2x} , A_{3x} , and A_{4x} depend on the conductivity coefficients σ_0 , ω_0 , T_2 , and S [23]. The explicit update for the magnetic field component is

$$H_z^{n+1/2}(i,k) = H_x^{n-1/2}(i,k) + \frac{\Delta t}{\mu_0} \left[\frac{E_y^n(i + \frac{1}{2},k) - E_y^n(i - \frac{1}{2},k)}{\Delta x} + \frac{E_x^n(i,k + \frac{1}{2}) - E_x^n(i,k - \frac{1}{2})}{\Delta y} \right]. \quad (5)$$

Equations (2) and (5) constitute the complete FDTD time-stepping algorithm for a Lorentzian dispersive medium with optical gain. This algorithm is second-order accurate in space and time increments, and it reduces to the normal FDTD update equations when $T_2=0$.

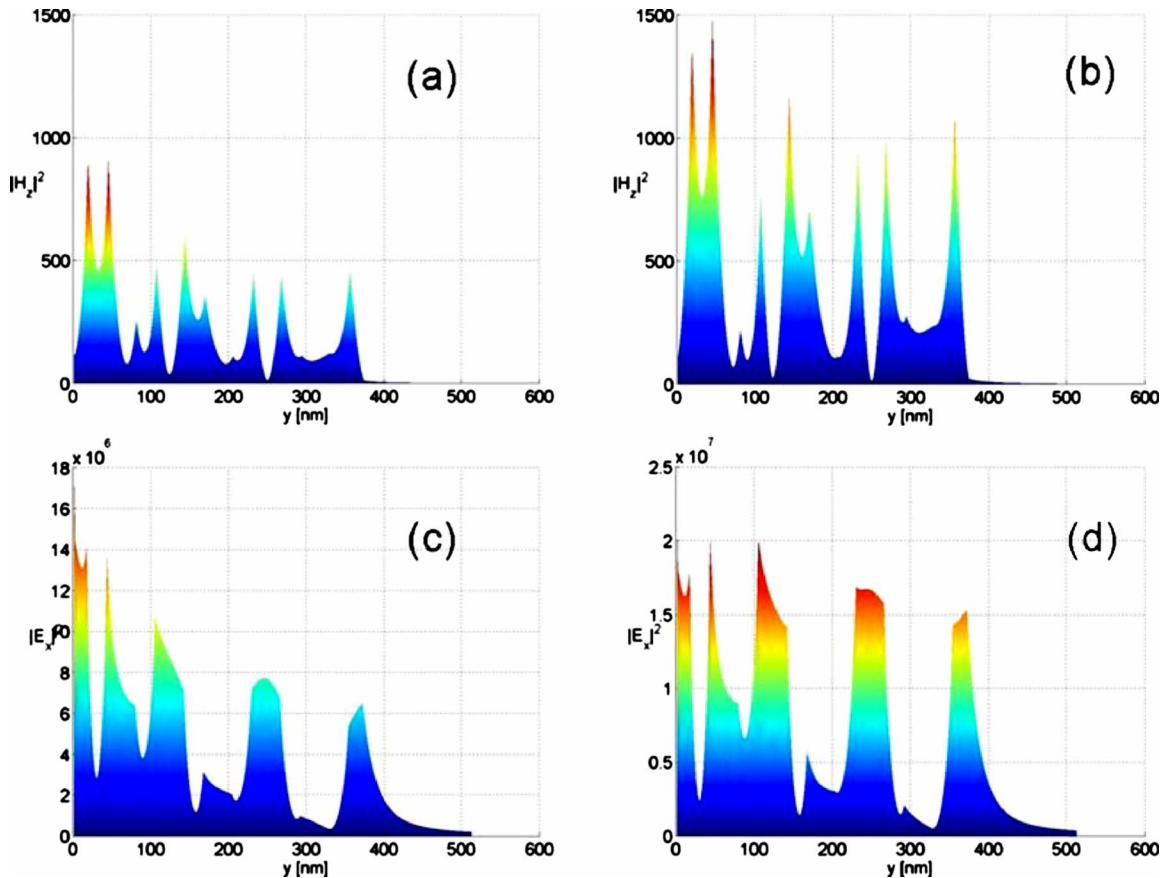


FIG. 6. (Color online) Effects of gain introduction of field localization inside the multilayer. Both the (b) electric and (d) magnetic fields in the presence of gain exhibit stronger values than both fields in the passive structure (a) and (c).

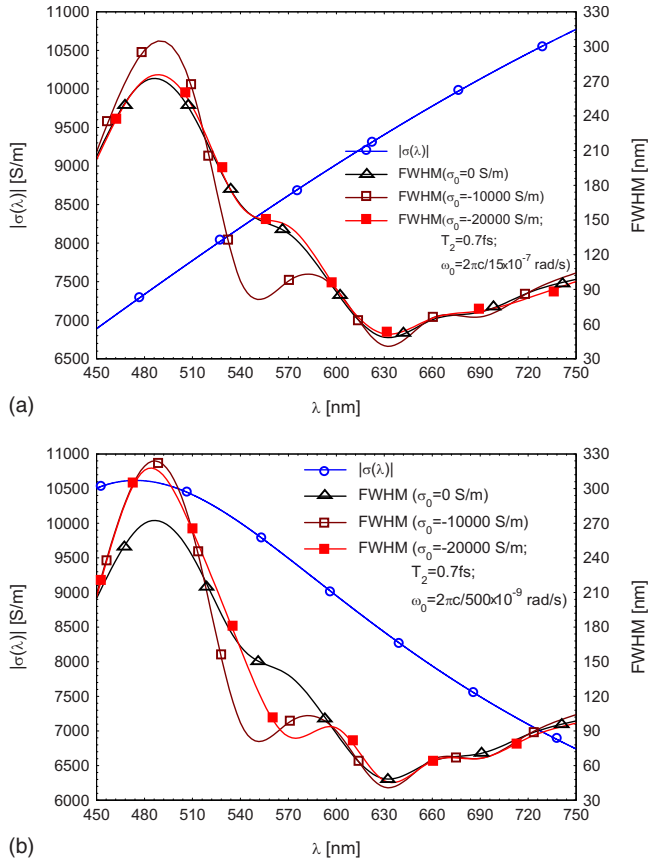


FIG. 7. (Color online) (a) FWHM against incident wavelength for increasing gain profile and (b) FWHM as a function of the incident wavelength for decreasing gain profile. The spot size (FWHM) of the Poynting vector not only depends on the modulus of σ . The minimum spot size is achieved near 630 nm in both cases.

III. RESONANT METAL-DIELECTRIC STRUCTURE WITH OPTICAL GAIN

The structure under investigation is a multilayer stack composed of 5.5 Ag/X periods, whose elementary cell has a

26-nm-thick Ag layer and a 36-nm-thick layer of material X. The entry and exit surfaces of the structure are coated with two layers of material X 18 nm thick (Fig. 1). The dispersion profile of silver is found in Palik's handbook [24], while for the sake of simplicity material X is assumed to be a dispersion-free lossless dielectric material with refractive index $n=4$. It has been demonstrated previously that these restrictions on the dielectric material can be removed with minimal impact on both qualitative and quantitative aspects of the performance of the lens [6]. The plane-wave transmittance, reflectance, and absorbance of this system are calculated by means of the transfer matrix method at 45° of incidence with respect to the propagation direction (see Fig. 2): the stack exhibits high transmittance and near-zero reflectance in a wavelength range that covers a large part of the visible spectrum, from 480 to 760 nm, in spite of the inclusion of 132 nm of silver. The source input has been simulated by carving a 24 nm aperture in an opaque germaniumlike substrate 200 nm thick. However, the choice of an opaque germaniumlike screen [7] is by no means unique and is used to mimic the behavior of a realistic source also providing a possible guide for experiments.

In order to compare and contrast the behavior of the passive structure with the active one we considered different gain profiles. The first amplification profile considered has a constant shape equivalent to imposing $\sigma_0 = -G$, where G is the maximum gain value. In order to implement this gain profile one must also impose $T_2 = 0$ and $\omega_0 = 0$ so that from Eq. (1) it results in $\sigma(\omega) = \sigma_0 = -G$. Even if these conditions are far from realistic (flat gain profile), this amplification profile was studied to understand the effects of the amplification mechanism on the balancing act the electromagnetic momentum plays inside the stack. Three different values of G are reported in Fig. 3: -2500 , -5000 , and -10000 S/m. Figure 3 clearly shows how the peak value of the longitudinal Poynting vector increases with the modulus of G , exhibiting two frequencies ($\lambda = 630$ nm and $\lambda = 570$ nm) where the effects of gain are particularly important.

Together with the exit power, the full width at half maximum (FWHM) at the exit surface of the stack also provides

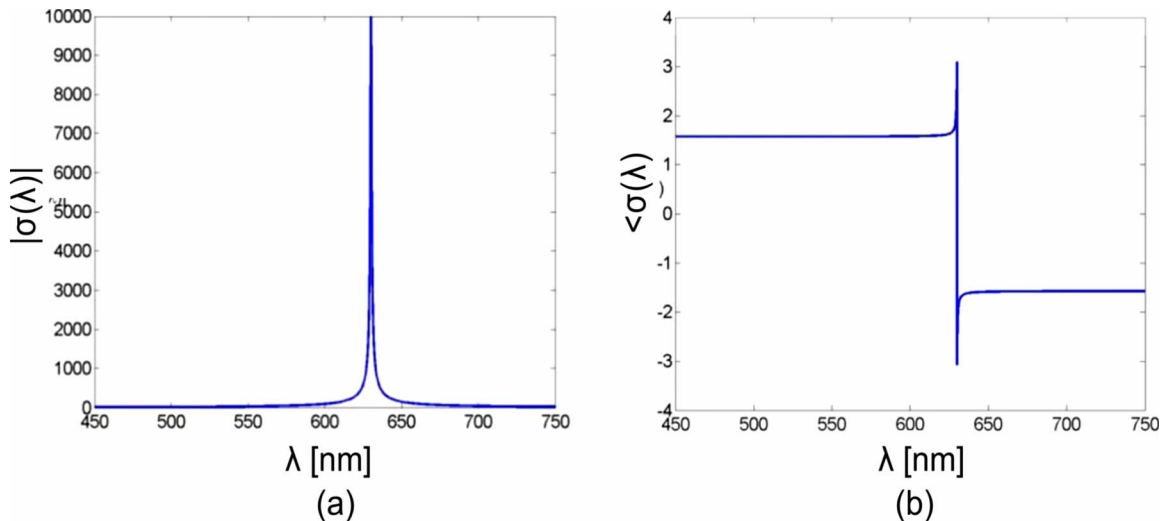


FIG. 8. (Color online) (a) Modulus and (b) phase of the conductivity. The parameter of Eq. (1) has been set to $\sigma_0 = -20000$ S/m, $T_2 = 0.7$ ps, and $\omega_0 = 2\pi c / (630 \times 10^{-9})$ rad/s.

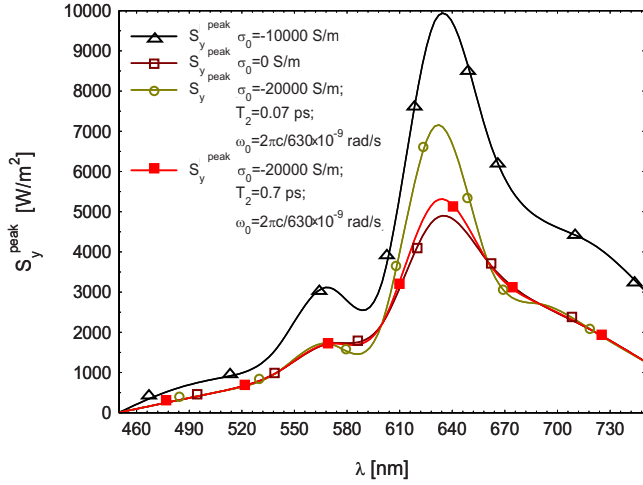


FIG. 9. (Color online) Peak value of the longitudinal Poynting vector at the exit of the stack as a function of the wavelength and for different gain profiles. The comparison of these curves reveals the strong dependence of the enhancement of the exit power on the parameter T_2 .

important information about the compensation of the diffraction process due to the presence of gain. In Fig. 4 we report the FWHM of the longitudinal Poynting vector as a function of wavelength while noting a detriment to field confinement for $450 \text{ nm} < \lambda < 510 \text{ nm}$ and $\lambda > 720 \text{ nm}$. It is also worth noting that in these regions of the spectrum the peak power (Fig. 3) does not undergo significant improvements. At the same time we report that for other wavelengths the diffraction process is limited by the presence of gain. For instance, at $\lambda = 630 \text{ nm}$ we obtain a FWHM of $\sim 41 \text{ nm}$ at the exit of the stack, with a reduction of $\sim 7 \text{ nm}$ with respect to the passive structure. At this frequency we also register the maximum transmitted power for the longitudinal Poynting vector (Fig. 3). For the sake of completeness the longitudinal Poynting vector profile at the exit of the stack for an incident

wavelength $\lambda = 630 \text{ nm}$ and different constant gain profiles is depicted in Fig. 5: the presence of gain improves the formation of the negative lobes around the central channel, meaning that the amplification also influences evanescent modes and thus the formation of surface waves at metal-dielectric interfaces and thus helping with ousting the suppression of diffraction inside the stack. Figure 6 illustrates a transverse section of the stack where we compare field localization inside the dielectric layers in the passive structure and following the introduction of gain.

Since the suppression of the diffraction process is not merely a problem of power but strongly depends on the balancing of the total momentum inside the stack, the inclusion of materials having disproportionate values of gain could indeed result in a detrimental effect on field confinement. In fact considering values of G greater in magnitude than $15\,000 \text{ S/m}$, the longitudinal component of the Poynting vector achieves a FWHM greater than 500 nm for a 24-nm -wide source.

Following this analysis is the inclusion of gain profiles $\sigma(\omega)$ having nonuniform (increasing and then decreasing) features. In order to correctly compare the peak value of $\sigma = -10\,000 \text{ S/m}$ we considered a peak value of $\sigma_0 = -20\,000 \text{ S/m}$, $T_2 = 0.7 \text{ fs}$, and in turn $\omega_0 = 2\pi c / (1500 \times 10^{-9}) \text{ rad/s}$ for the increasing profile and $\omega_0 = 2\pi c / (500 \times 10^{-9}) \text{ rad/s}$ for a decreasing profile. As shown in Fig. 7, the FWHM of the longitudinal Poynting vector at the exit of the stack preserves its minimum spectral position at $\lambda \sim 630 \text{ nm}$ although at this wavelength an appropriate peak amplitude for $\sigma(\lambda)$ and slope may decrease spot size by $40\text{--}50 \%$.

In order to simulate a more realistic material we considered different resonant gain profiles having the same peak value σ_0 and by varying the resonance frequency and the time constant T_2 . Figure 8 depicts the modulus and the phase of the conductivity for the first case considered, having a resonant wavelength tuned at 630 nm so that $\omega_0 = 2\pi c / (630 \times 10^{-9}) \text{ rad/s}$ and $T_2 = 0.7 \text{ ps}$. Different from

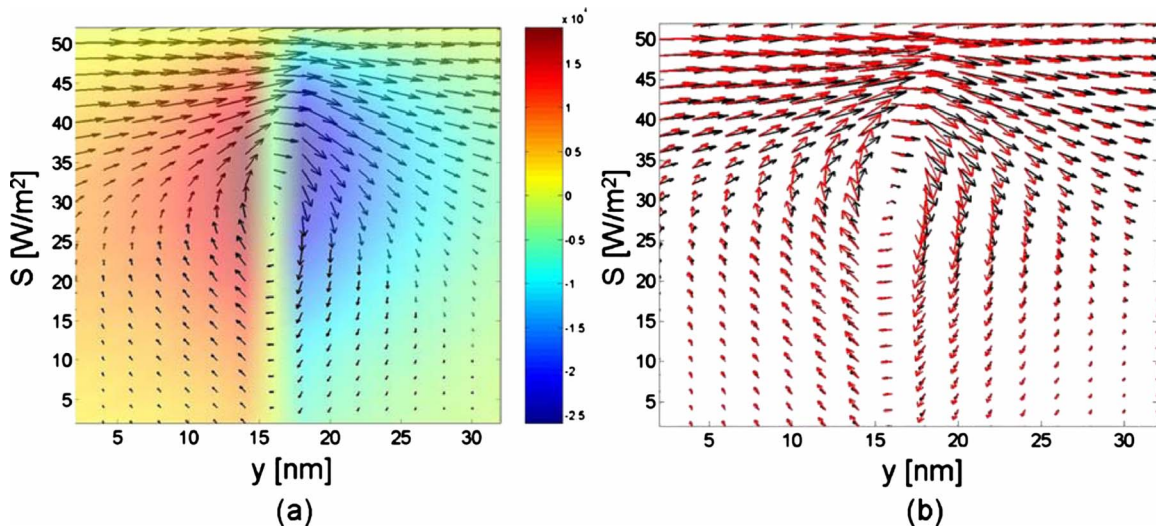


FIG. 10. (Color online) (a) Vortex formation at a dielectric/metal interface inside the passive stack and (b) comparison in the vortex formation and Poynting vector intensity without (black/dark gray arrows) and with (red/light gray arrows) gain. The incident wavelength is tuned at $\lambda = 630 \text{ nm}$ and a constant gain profile with $\sigma_0 = -10\,000 \text{ S/m}$ is considered.

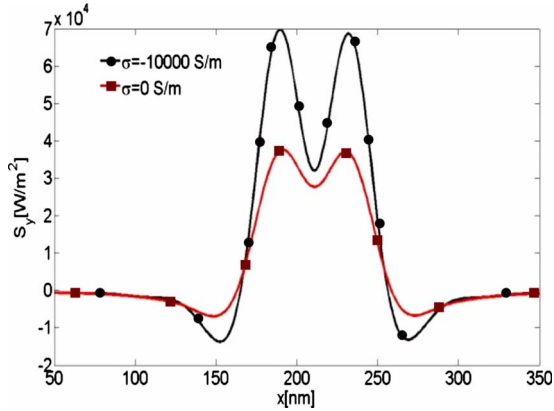


FIG. 11. (Color online) Longitudinal components of the Poynting vector at the exit of the stack when two 52-nm-wide slits have been carved on an opaque germaniumlike substrate. The center-to-center distance between the slits is 86 nm.

the cases of constant, increasing, and decreasing gain profiles discussed above, no significant variations were registered in the FWHM of the longitudinal Poynting vector, while small improvements are noted in the exit power.

By simply scaling down the time constant, which corresponds to enlarge the resonant peak in the amplification profile, we obtained a significantly different response at the exit of the stack: even if the FWHM does not exhibit meaningful improvements, by setting $T_2=0.07$ ps, the peak power of the longitudinal Poynting vector at the exit surface is enhanced around the resonant frequency with respect with the passive case and the resonant profile with a narrower resonance (Fig. 9).

Since the spectral distribution of the amplification has significant impact on the peak power at the exit of the stack, we then analyzed wavelengths where the multilayer does not confine the light efficiently. We considered the following parameters for the conductivity equation: $\sigma_0=-20\,000$ S/m, $T_2=0.07$ ps, and $\omega_0=2\pi c/(720\times 10^{-9})$ rad/s. Shifting the resonance frequency to 720 nm we obtained some improvements in the transmitted power and in field confinement: under these conditions the peak of the Poynting vector at the exit of the stack approaches the values obtained for the constant gain profile with $\sigma(\omega)=-10\,000$ S/m. Moreover, the FWHM at $\lambda=720$ nm and surrounding wavelengths undergoes a modest reduction of ~ 3 nm with respect to the passive case and the constant gain profile.

As was the case for the passive device, the variation of the FWHM for different source sizes could provide important information about the capacity of the stack to suppress the diffraction process. For the sake of simplicity we compared two apertures (12 and 24 nm wide) carved on a germanium-like substrate considering two different gain profiles: (i) constant with $\sigma_0=-10\,000$ S/m and (ii) resonant profile with $\sigma_0=-20\,000$ S/m, $T_2=0.07$ ps, and $\omega_0=2\pi c/(720\times 10^{-9})$ rad/s. This analysis revealed that the best field confinement is still obtained at $\lambda=630$ nm, independent of gain profile. Moreover, at $\lambda=635$ nm the structure produces the same image at the exit of the stack for both aperture sizes, meaning that this condition may be favorable for the super-resolution regime.

IV. POYNTING VECTOR VORTICITY AND SUPER-RESOLUTION IMPROVEMENT FOLLOWING THE INTRODUCTION OF GAIN

Metal-dielectric multilayer photonic band gap structures have been demonstrated to have the impressive capabilities to guide and confine light as well as suppress the diffraction process, culminating in super-resolution in the visible range [6]. This kind of performance is primarily due to the resonant nature of these stacks, which in the resonance tunneling regime are able to efficiently transport propagating and evanescent modes impinging from subwavelength apertures. Negative refraction occurring inside the metal layers is nearly balanced by positive refraction occurring inside the dielectric materials. This alternation also causes the propagation of surface waves at each interface that under certain conditions could result in the formation of vortices both inside and immediately outside the stack [6,25]. Since the introduction of gain modifies dielectric properties, the formation of surface plasmons and vortices is also altered compared to the passive case. For simplicity we once again considered a constant gain profile with $\sigma(\omega)=-10\,000$ S/m and an impinging wavelength tuned at $\lambda=630$ nm. By looking at a dielectric/metal interface inside the stack we can easily distinguish the differences between these two materials by simply observing the local direction of the Poynting vector [direction of arrows in Fig. 10(a) refers to the passive stack]. As depicted in Fig. 10(b), the introduction of gain significantly modifies both the intensity and the direction of the Poynting vector.

The improvement of the vorticity of the Poynting vector following the introduction of gain also suggests that the super-resolution may be enhanced. As stated in the previous paragraph, the wavelength that provides a better response in terms of super-resolution is $\lambda=635$ nm since the structure at this wavelength is not sensitive to source size and produces also the minimum spot size at the exit interface.

We considered two 52-nm-wide slits carved in the opaque realistic germaniumlike substrate. The center-to-center distance between the slits was fixed to 86 nm. By comparing the longitudinal Poynting vector profile for a passive and an active stack [constant gain profile is considered with $\sigma(\omega)=-10\,000$ S/m] we noticed a boost in the resolving ability of the lens, going from a visibility of $\sim 15\text{--}\sim 37\%$ when the active dielectric material is considered (Fig. 11).

V. CONCLUSIONS

We have shown the properties of a resonant metal-dielectric stack when the dielectric material is replaced with an active one. Different gain profiles were considered in order to highlight the dependence of superguiding and super-resolution abilities as functions of incident wavelength. The improvement of both vorticity and resolution was demonstrated in the case of constant gain profile. The introduction of such gain indeed helps the super-resolution process, enhancing the lens peculiarities also for wavelengths where lens performance is frustrated.

ACKNOWLEDGMENT

The authors thank the U.S.-Army European Research Office for partial financial support.

- [1] J. B. Pendry, Phys. Rev. Lett. **85**, 3966 (2000).
- [2] D. O. S. Melville and R. J. Blaikie, Opt. Express **13**, 2127 (2005); N. Fang, H. Lee, C. Sun, and C. X. Zhang, Science **308**, 534 (2005).
- [3] Z. Liu, H. Lee, Y. Xiong, C. Sun, and X. Zhang, Science **315**, 1686 (2007).
- [4] S. Anantha Ramakrishna, J. B. Pendry, M. C. K. Wiltshire, and W. J. Stewart, J. Mod. Opt. **50**, 1419 (2003).
- [5] M. Scalora, M. J. Bloemer, A. S. Manka, S. D. Pethel, J. P. Dowling, and C. M. Bowden, J. Appl. Phys. **83**, 2377 (1998).
- [6] D. de Ceglia, M. A. Vincenti, M. G. Cappeddu, M. Centini, N. Akozbek, A. D’Orazio, J. W. Haus, M. J. Bloemer, and M. Scalora, Phys. Rev. A **77**, 033848 (2008).
- [7] M. Scalora, G. D’Aguanno, N. Mattiucci, M. J. Bloemer, D. de Ceglia, M. Centini, A. Mandatori, C. Sibilina, N. Akozbek, M. G. Cappeddu, M. Fowler, and J. W. Haus, Opt. Express **15**, 508 (2007).
- [8] M. Bloemer, G. D’Aguanno, N. Mattiucci, M. Scalora, and N. Akozbek, Appl. Phys. Lett. **90**, 174113 (2007).
- [9] T. J. Yen, W. J. Padilla, N. Fang, D. C. Vier, D. R. Smith, J. B. Pendry, D. N. Basov, and X. Zhang, Science **303**, 1494 (2004).
- [10] S. Linden, C. Enkrich, M. Wegener, J. Zhou, T. Koschny, and C. M. Soukoulis, Science **306**, 1351 (2004).
- [11] R. A. Shelby, D. R. Smith, and S. Schultz, Science **292**, 77 (2001).
- [12] G. Dolling, C. Enkrich, M. Wegener, J. F. Zhou, C. M. Soukoulis, and S. Linden, Opt. Lett. **30**, 3198 (2005).
- [13] V. M. Shalaev, W. Cai, U. K. Chettiar, H. Yuan, A. K. Sarychev, V. P. Drachev, and A. V. Kildishev, Opt. Lett. **30**, 3356 (2005).
- [14] U. K. Chettiar, A. V. Kildishev, H.-K. Yuan, W. Cai, S. Xiao, V. P. Drachev, and V. M. Shalaev, Opt. Lett. **32**, 1671 (2007).
- [15] V. M. Shalaev, Nat. Photonics **1**, 41 (2007); G. Dolling, C. Enkrich, M. Wegener, C. M. Soukoulis, and S. Linden, Opt. Lett. **31**, 1800 (2006).
- [16] G. Dolling, M. Wegener, C. M. Soukoulis, and S. Linden, Opt. Lett. **32**, 53 (2007).
- [17] S. Anantha Ramakrishna and J. B. Pendry, Phys. Rev. B **67**, 201101(R) (2003).
- [18] B. Wood, J. B. Pendry, and D. P. Tsai, Phys. Rev. B **74**, 115116 (2006).
- [19] P. A. Belov and Y. Hao, Phys. Rev. B **73**, 113110 (2006).
- [20] K. Ohtaka, J. Lightwave Technol. **17**, 2161 (1999).
- [21] A. D’Orazio, V. De Palo, M. De Sario, V. Petruzzelli, and F. Prudenzano, PIER **39**, 299 (2003).
- [22] S. Nojima, Jpn. J. Appl. Phys. **37**, 6418 (1998).
- [23] A. Taflove and S. Hagness, *Computational Electrodynamics: The Finite-Difference Time-Domain Method*, 3rd ed. (Artech, Norwood, MA, 2005).
- [24] E. D. Palik, *Handbook of Optical Constants of Solids* (Academic Press, New York, 1985), Vol. I, pp. 353–357.
- [25] G. D’Aguanno, N. Mattiucci, M. Bloemer, and A. Desyatnikov, Phys. Rev. A **77**, 043825 (2008).